ANL/TD/TM00-13

Technology Development Division
Technology Development Division
Technology Development Division

The Effect of Laser Welding Process Parameters on the Mechanical and Microstructural Properties of V-4Cr-4Ti Structural Materials[§]

by
Claude Reed, Ken Natesan, Zhiyue Xu, and Dale Smith

Argonne National Laboratory, Argonne, Illinois 60439
operated by The University of Chicago
for the United States Department of Energy under Contract W-31-109-Eng-38

Fusion Power Program

Available electronically at http://www.doe.gov/bridge

Available for a processing fee to U.S. Department of Energy and its contractors, in paper, from:

U.S. Department of Energy
Office of Scientific and Technical Information
P.O. Box 62
Oak Ridge, TN 37831-0062
phone: (865) 576-8401
fax: (865) 576-5728
email: reports@adonis.osti.gov

May 2000 ANL/TD/TM00-13

THE EFFECT OF LASER WELDING PROCESS PARAMETERS ON THE MECHANICAL AND MICROSTRUCTURAL PROPERTIES OF V-4Cr-4Ti STRUCTURAL MATERIALS§

C. B. Reed, K. Natesan, Z. Xu, and D. L. Smith

Argonne National Laboratory
9700 South Cass Avenue
Argonne, IL 60439

Work supported by the
Office of Fusion Energy Sciences
U.S. Department of Energy
Under Contract W-31-109-ENG-38

CONTENTS

THE EFFECT OF LASER WELDING PROCESS PARAMETERS ON THE MECHANICAL AND MICROSTRUCTURAL PROPERTIES OF V-4Cr-4Ti STRUCTURAL MATERIALS§

C. B. Reed, K. Natesan, Z. Xu, and D. L. Smith

Fusion Power Program, Argonne National Laboratory
9700 S. Cass Ave., Argonne, IL 60439, USA
Telephone: ++1 630 252-5970, FAX: ++1 630 252 5287, E-mail: cbreed@anl.gov

ABSTRACT

This paper reports on a systematic study which was conducted to examine the use of a pulsed Nd:YAG laser to weld sheet materials of V-Cr-Ti alloys and to characterize the microstructural and mechanical properties of the resulting joints. Deep penetration and defect-free welds were achieved under an optimal combination of laser parameters including focal length of lens, pulse energy, pulse repetition rate, beam travel speed, and shielding gas arrangement. The key for defect-free welds was found to be the stabilization of the keyhole and providing an escape path for the gas trapped in the weld. An innovative method was developed to obtain deep penetration and oxygen contamination free welds. Oxygen and nitrogen uptake were reduced to levels only a few ppm higher than the base metal by design and development of an environmental control box. Effort directed at developing an acceptable postwelding heat treatment showed that five passes of a diffuse laser beam over the welded region softened the weld material, especially in the root region of the weld.

INTRODUCTION

V-Cr-Ti alloys are among the leading candidate materials for the first wall and other structural materials applications in fusion power reactors because of several important advantages including inherently low irradiation-induced activity, good mechanical properties, good compatibility with lithium, high thermal conductivity and good resistance to irradiation-induced swelling and damage [1]. However, weldability of these alloys in general must be demonstrated, and laser welding, specifically, must be developed. Laser welding is considered to be an attractive process for construction of a reactor due to its high penetrating power and potential flexibility.

To address these issues, a systematic study was conducted to examine the use of a pulsed Nd:YAG laser to weld sheet materials of V-Cr-Ti alloys and to characterize the microstructural and mechanical properties of the resulting joints. Vanadium alloy heat #832665, nominal composition V-4 wt% Cr-4 wt% Ti (designated as BL-71) was selected for the study. Bead-on-plane (BOP) welds were produced on 4 mm thick sheets of the alloy using a 1.6 kW pulsed Nd:YAG laser with optical fiber beam delivery. The effects of laser parameters on depth of penetration, oxygen and nitrogen uptake, and

microhardness, were determined experimentally. The three main tasks of the study were to:

(a) Determine the optimal parameters for full penetration, defect-free, laser beam welding of 4mm thick sheets of V-Cr-Ti alloys, and examine the microstructural characteristics of the welded sections, including base metal, heat-affected-region, and core of the weld.

(b) Determine the extent of oxygen uptake from the welding process, its influence on weld joint hardness, and minimize it.

(c) Evaluate the influence of different postwelding heat treatments on microstructural characteristics and local hardness profiles.

STUDIES TO INCREASE DEPTH OF PENETRATION

Group I

An initial run of seven identical welds, produced for subsequent heat treating studies and labeled 1H-7H, provided the starting point[2]. For these welds, laser beam power was 1325 W and travel speed was 110 mm/s. A 127 mm (5") focal length lens was used, and the focus was 1 mm into the material. The beam was 1 mm in diameter and penetration was 1.4 mm into the 4-mm-thick sheet. An argon shielding gas was used with a flow rate of 0.25 L/s, provided by a 9.5-mm-diameter tube at 30° from horizontal. The welds were started and ended on a scrap piece of vanadium so that penetration depth could be seen at both ends of the weld. The vanadium plate was clamped to an aluminum plate, which in turn was clamped to a water-cooled copper block; this arrangement provided sufficient cooling to keep the vanadium sheet barely warm after welding. Group I laser welding parameters are summarized in Table 1.

Figure 1 contains an SEM photomicrograph of the cross section of Weld 3H specimen in the as-welded condition. The weld has a substantial variation in grain size from the root of the weld to the free surface region. Also, the grains near the top of the weld are columnar, which is dictated by rate of cooling and solidification. Even in the root of the weld, the grains are of the order of two to five times larger than those of the base metal away from the weld. Further, the weld cross section shows definite contours evenly spaced in the root region, along which can occur preferential segregation of impurities. The dark- and light-shaded grains in the weld are due to differences in grain orientation; virtually no compositional variations were observed between these grains.

In the Weld 3H specimen, Knoop hardness measurements were made at three different elevations and on both sides of the weld centerline. These elevations are designated by A, AA, B, BB, C, and CC, as shown in Figure 1. Knoop hardness profiles at different elevations are also shown in Figure 1 and indicate that the hardness values on either side of the weld centerline were similar at all three elevations examined. The hardness profiles at elevation A and AA indicate a peak value of 270 in the weld zone, while the

base metal had values of 165 to 190. At weld elevations B and BB, the weld pool zone had a hardness value of 250 at a depth of 0.35-0.40 mm, beyond which hardness dropped monotonically to base metal values of 170-190. At elevations C and CC, the hardness profiles indicated a drop in the weld centerline region from 250 to 190-215, while a peak in hardness was noted at a distance of 0.8-0.9 mm from the weld centerline. Hardness profiles of the weld specimen in Figure 1 showed that the profiles are symmetrical on either side of the weld centerline.

Group II

To increase penetration from 1.3 mm, typical of welded samples 1H-7H of Group I, to as deep as 3 mm or more, welding parameters such as power, traverse speed, pulse time, overlap, etc., were examined in Group II to obtain optimal quality in the final weld[3]. For Group II welds, the energy of the laser beam was increased to values of 4.5-5.5 J/ms; pulse width was maintained at 3 ms. Additionally, workpiece traverse speed was varied between 10 and 40 mm/s. For Groups II, III, and IV, high-purity argon (99.999%) was used as the shielding gas with a flow rate of 0.42 L/s, provided by a 9.5-mm diameter tube at 30° from horizontal.

Table 2 summarizes welding parameters used and results obtained, including work piece traverse speed and penetration depths for four different welds in Group II (identified as AP, BP, CP, and DP) which were made with laser energy in the range of 5.2-5.5 J/ms. Weld AP, with a shallower penetration, exhibited almost no porosity, and no undue material transfer to the weld surface was noted. Figure 2 shows a low-magnification photomicrograph of weld AP. Welds BP, CP, and DP, with somewhat deeper penetration, exhibited root porosity in the weld as shown in Figure 3 for weld DP, which is typical of the others. The cause of this root porosity and the adjustments to welding parameters to eliminate this defect were studied in the Group III welds.

Six additional Group II welds (identified as 1P, 2P, 3P, 4P, 5P, and 6P in Table 2) were made with laser energy of 4.5 J/ms; pulse width was maintained at 3 ms. Examination of the weld cross sections showed that 4P, 5P, and 6P had almost no macroporosity, but 1P, 2P, and 3P exhibited significant root porosity. Figure 4 shows low-magnification photomicrographs of weld 3P (typical of 1P, 2P, and 3P) and weld 5P (typical of 4P, 5P, and 6P). Two conclusions can be drawn from the Group II welds. First, to increase the depth of penetration of the weld, the laser energy must be higher; it is evident that the higher energy used for welds AP-DP resulted in deeper penetration than the lower power used for welds 1P-6P. Second, the traverse speed of the workpiece seems to have an effect (which may not display a 1:1 correlation) on development of root porosity in the welds. For example, welds 1P-3P (made with a traverse speed of 40 mm/s) showed defects, while welds 4P-6P (with a traverse speed of 30 mm/s) exhibited no defects. On the other hand, weld AP (made with a laser energy of 5.2 J/ms and traverse speed of 30 mm/s) was defect-free, while welds BP and CP, (made with the same laser energy and traverse speeds of 20 and 25 mm/s) exhibited defects.

In all the Group II welds (AP-DP and 1P-6P), variation in grain size from the root of the weld to the free-surface region was lower than that observed in Group I welds. Also, in

the Group I welds, the grains near the top of the weld were columnar, which is dictated by rate of cooling and solidification, but such a structure was confined to only the center region in the Group II welds. Further, the Group II weld cross sections shows definite contours evenly spaced in the root region, similar to those observed in Group I welds. The dark- and light-shaded grains in the Group II welds are due to differences in grain orientation; and, like the Group I welds, virtually no compositional variations were observed between these grains.

Vickers hardness measurements were made on Group II defect-free weldments AP, 4P, 5P, and 6P, in the surface-to-root direction and from the centerline of the weld toward the base metal at half-width of the weld. Figure 5 shows the hardness profiles for these welds in the two directions. The results indicate that in three of the four (specimens AP, 4P, and 6P) weldments, the hardness value gradually decreases from 200-210 in the centerline of the weld to 160 in the base metal over a distance of 0.4-0.5 mm from the weld centerline. In these three weldments, hardness was fairly constant in the range of 200-210 from the surface-to-root direction, after which a sharp drop in hardness is noted. Weldment 5P exhibited unusually high hardness in both directions, the cause for which is not known at present.

Group III

For the Group III study, thirty eight weldments were made with the Nd:YAG laser; the emphasis was on determining the optimal weld parameters to achieve deeper penetration in the welds while eliminating porosities found in Group II welds[4]. A preliminary assessment was then made of the weldments on the basis of visual appearance and sectioning to determine depth of penetration and extent of porosity. The main purpose of these 38 runs was to obtain ideal welds which had enough penetration for Charpy impact specimens (weld depth > 2.74 mm) but no root porosity, surface splatter, or plate-out. Two different focal length lenses 127mm and 76mm were tested under different laser parameters and beam travel speeds. High-purity argon (99.999%) was used as the shielding gas with a flow rate of 0.42 L/s, provided by a 9.5-mm diameter tube at 30° from horizontal. The Group III series of welds are listed in Tables 3 and 4.

The Group III welds were metallurgically analyzed to characterize the weld depths and the microstructures. Root porosity was found in welds produced under relatively high beam travel speeds. Porosity was examined at a single, randomly selected cross section via 400X optical microscopy. The results of this porosity examination are summarized in Tables 3 and 4. Splatters were generated when the peak power of the laser beam was too high. Ideal welds (no porosity or irregular surface, and weld depth>2.74 mm) were achieved for each of the following three conditions:

Condition	Schedule	Lens	Beam travel speed
1	E4L3R132	127 mm	<= 1 cm/s
2	E4L3R132	76 mm	<= 1.5 cm/s
3	E5.2L3R102	76 mm	<= 2 cm/s

Ideal welds produced using the 127mm lens and the 76mm lens are shown in Figures 6 and 7, respectively.

Group IV

Based on the results of Group III welds, it was decided, for Group IV welds, to fix all parameters except beam travel speed, in pursuit of full penetration, defect-free welds[5]. Group IV consisted of four welds; all of which were EDM wire cut longitudinally along their centerlines to comprehensively examine for porosity. Cross-sectioned weld samples do not reveal completely the existence of porosity, since the randomly chosen section could be located just between porosities. Table 5 lists the welding conditions and weld depths of the four samples used to examine for porosity in longitudinal sections. A side view of the longitudinal section of all four welds is shown in Figure 8. Detailed views of individual sections are presented in Figures 9 to 12. It can be seen that the amount of porosity decreases as the beam travel speed decreases. Porosity-free welds were obtained when the weld depth reached full penetration. Group IV results seem to show that full penetration provides a path on the bottom side of the sample for the gas trapped in the welding keyhole to escape, thus eliminating porosity.

STUDIES TO MINIMIZE CONTAMINATION

Group V

With full penetration and defect-free welding accomplished, attention was turned, in Group V, to weld purity issues, starting with oxygen, carbon, and nitrogen uptake during processing[5]. Uptake of oxygen leads to embrittlement of the alloy and therefore must be avoided. For Group V, the laser schedule was fixed, as in Group IV, at schedule E4L3R132. With beam travel speed, lens, and shielding gas flow identical to weld #1 in Group IV, two weld specimens, 990223B (23B) and 990223C (23C), were produced and the core of each weld was machined into chips and analyzed for O, C, and N. The content of oxygen, nitrogen, and carbon of laser-welded samples was analyzed by the Inert Gas Fusion (IGF) method. Results of those analyses, along with analyses of the base material adjacent to the welds (specimen 23A), are shown in Figure 13. Also shown in Figure 13 for comparison purposes, are reference analyses of O, C, and N from the original Heat 823665, from which the 4mm sheets were produced. It can be seen that specimens 23B and 23C obviously exhibit unacceptably large amounts of oxygen and nitrogen.

A custom-designed environmental control box (ECB) capable of purging with high-purity argon (99.995%) was integrated with the Nd:YAG laser to improve the quality of the welding atmosphere by minimizing oxygen and nitrogen uptake. Figure 14 schematically shows the set-up of the laser system with the ECB. Specimens were placed in the ECB with fixtures. The high-purity argon was purged into the box from both sides and the flow rate was well controlled such that a slow flow of argon out from the slit on the top of the box could be formed This provided a good welding atmosphere to minimize the

impurity uptake during welding. A shielding disk just above the slit enhanced the shielding effect and also provided a guiding surface for the lens protection gas.

Figure 13 shows that the welds produced in the ECB with nearly optimal shielding gas (12B and 12C) have the lowest oxygen content. Welds using the ECB but with a less than optimal gas shielding arrangement (09A and 09B) have higher oxygen content compared to those with nearly optimal shielding. The welds obtained without using the ECB have the highest oxygen content. The specimens were wiped with acetone before and after welding except specimen 09B, which was cleaned in a pickling solution after welding. The O, N, and C contents of welds produced using the ECB with near-optimal shielding gas are essentially the same as the values reported as the reference analysis for the starting material. Oxygen analyses obtained from the chip samples (23B & 23C) apparently include additional contamination. Subsequent specimens were not milled into chips prior to chemical analysis, but rather submitted as small bars. By design and development of this environmental control box method, oxygen and nitrogen uptake were reduced to levels only a few ppm higher than the base metal.

A microhardness profile across the width of weldment 12D is presented in Figure 15. This profile shows only a slight increase in hardness in the weld metal, in comparison to the adjacent base metal.

EFFECT OF POST-WELD HEAT TREATMENT ON WELDMENT HARDNESS

For the post-weld heat treatment study, seven different welds (those produced in Group I) were made under the same welding conditions but were subsequently given different post-welding heat treatments[2]. The laser welding parameters are summarized in Table 1. Weld depth in these specimens was 1.2 mm and the hardness profiles generally show a substantial increase (from an initial Vickers hardness value of 170-180, up to 240-280) in the center of the weld; this value stays high across almost the entire weld zone, see Figure 1. The effort directed at developing an acceptable postwelding heat treatment showed that five passes of diffuse laser beam over the welded region softened the weld material, especially in the root region of the weld.

The heat treatments applied are listed in Table 6. Weld 3H remained in the as-welded condition. Welds 1H and 2H were given post-welding heat treatment of 1 and 5 passes, respectively, with a defocused beam. Welds 4H and 5H were post-welding heat treated with 50% of the power level of welds 1H and 2H. Welds 6H and 7H were treated with a power level of 25% of welds 1H and 2H. The defocused beams were wider than the welds (4 mm beam, compared to3 mm for the weld). Weld cross sections of different specimens were examined by scanning electron microscopy (SEM). In addition, Knoop hardness measurements were made at three different elevations across the width of the weld, starting at the weld centerline, through the heat-affected zone, and into base metal, see Figures 1, 16, and 17.

Figure 1 contains an SEM photomicrograph of the cross section of Weld 3H which was discussed earlier. Figure 16 includes an SEM photomicrograph of the cross section of a

welded specimen after post-welding heat treatment, designated as Weld 1H in Tables 1 and 6. As in the as-welded sample, this specimen showed a substantial variation in grain size from the root of the weld to the free surface region. Also, the grains near the top of the weld are columnar, dictated by rate of cooling and solidification. Figure 16 also shows the hardness profiles at elevations A, B, and C in the welded specimen. The effect of one pass of post-welding heat treatment with a defocused laser beam was to soften the material in the weld zone, as indicated by the monotonic decrease in hardness from the weld centerline to the base metal. Even the peak hardness value is somewhat lower and the peak is confined to the region close to the centerline. The impact of such a decrease on the mechanical properties of the weld can be substantial and will probably be beneficial.

Figure 17 shows an SEM photomicrograph of the cross section of a welded specimen after post-welding heat treatment, designated as Weld 2H in Tables 1 and 6. As in the previous samples, this specimen also shows that the weld has a substantial variation in grain size from the root of the weld to the free surface region. Also, the grains near the top of the weld are columnar in shape, again dictated by rate of cooling and solidification. Figure 17 also shows the hardness profiles at elevations A, B, and C in the welded specimen. The effect of five passes of post-welding heat treatment with a defocused laser beam was to soften the material in the weld zone, especially at the root region of weld. The erratic hardness variation in the weld region of this specimen at elevations B and C indicate that grain growth may have occurred in the upper portions of weld as a result of the multiple passes.

SUMMARY AND CONCLUSIONS

A systematic study was conducted to examine the use of a pulsed Nd:YAG laser to weld sheet materials of V-Cr-Ti alloys and to characterize the microstructural and mechanical properties of the resulting joints. Deep penetration and defect-free welds were achieved under an optimal combination of laser parameters including focal length of lens, pulse energy, pulse repetition rate, beam travel speed, and shielding gas arrangement. The key for defect-free welds was found to be the stabilization of the keyhole and providing an escape path for the gas trapped in the weld. An innovative method was developed to obtain deep penetration and contamination free welds. Oxygen and nitrogen uptake were reduced to levels only a few ppm higher than the base metal, by design and development of an environmental control box. The effort directed at developing an acceptable postwelding heat treatment showed that five passes of diffuse laser beam energy over the welded region softened the weld material, especially in the root region of the weld.

REFERENCES

1. H. M. Chung, J.-H. Park, R. V. Strain, K. H. Leong, and D. L. Smith, "Mechanical properties and microstructural characteristics of laser and electron-beam welds in V-4Cr-4Ti," J. Nucl. Mater. 258-263 (1998) 1451-1457.

2. K. Natesan, D. L. Smith, P. G. Sanders, and K. H. Leong, "Laser-Welded V-Cr-Ti Alloys: Microstructural and Mechanical Properties," Fusion Reactor Materials Progress Report for the Period Ending December 31, 1997, Argonne National Laboratory, DOE/ER-0313/23, p. 136, March 1998.

3. K. Natesan, D. L. Smith, Z. Xu, and K. H. Leong, "Laser-Welded V-Cr-Ti Alloys: Microstructural and Mechanical Properties,"Fusion Reactor Materials Progress Report for the Period Ending June 30, 1998, Argonne National Laboratory, DOE/ER-0313/24, p. 87, September, 1998.

4. K. Natesan, C. B. Reed, Z. Xu, and D. L. Smith, "Laser-Welded V-Cr-Ti Alloys: Microstructural and Mechanical Properties,"Fusion Reactor Materials Progress Report for the Period Ending December 13, 1998, Argonne National Laboratory, DOE/ER-0313/25, p. 64, April, 1999.

5. Z. Xu, C. B. Reed, K. Natesan, and D. L. Smith, "Improvement of Laser Weld Quality of V-Cr-Ti Alloys," Fusion Reactor Materials Progress Report for the Period Ending June 30, 1999, Argonne National Laboratory, DOE/ER-0313/26, p. 49, September, 1999.

Work supported by the Office of Fusion Energy Sciences, U.S. Department of Energy, under Contract No. W-31-109-ENG-38.

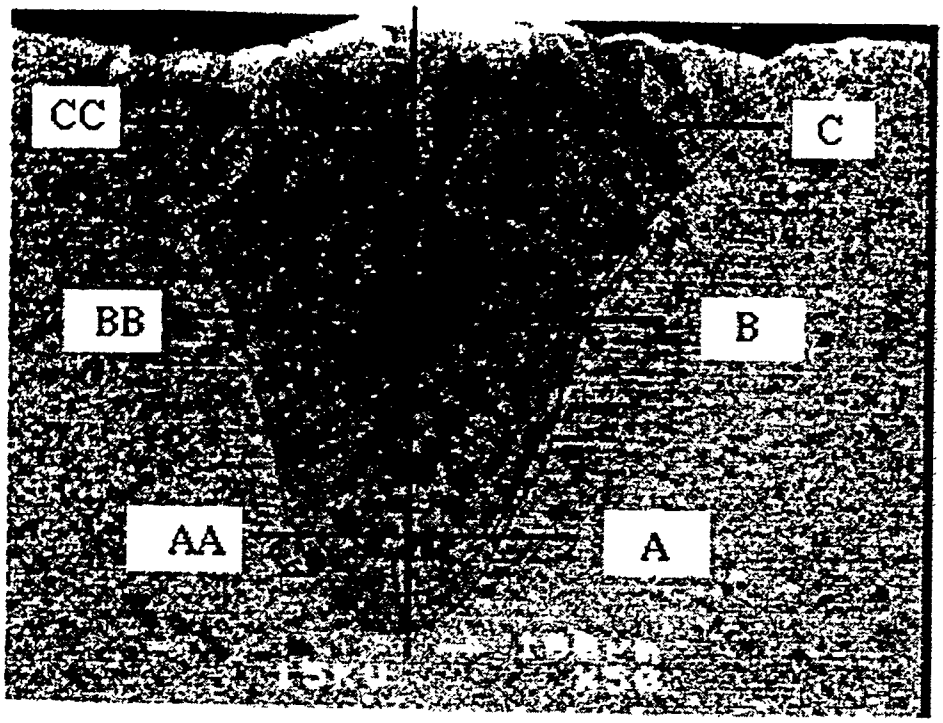

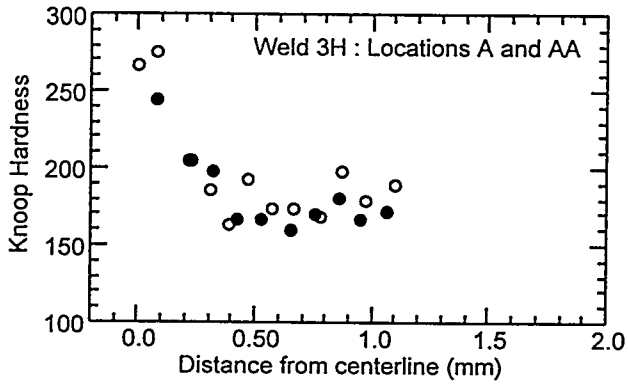

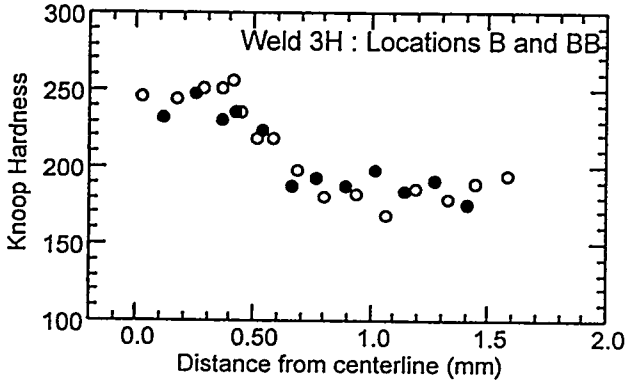

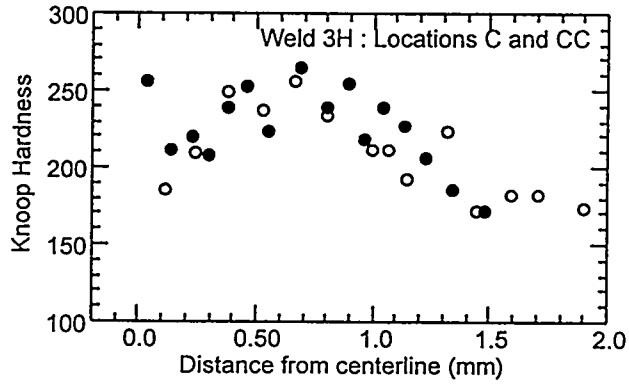

Figure 1. Hardness profiles at elevations indicated in photomicrograph for laser-welded V-4Cr-4Ti specimen from Group I, in as-welded condition, designated as Weld 3H in Table 1. Open and closed symbols represent hardness values measured on either side of weld centerline.

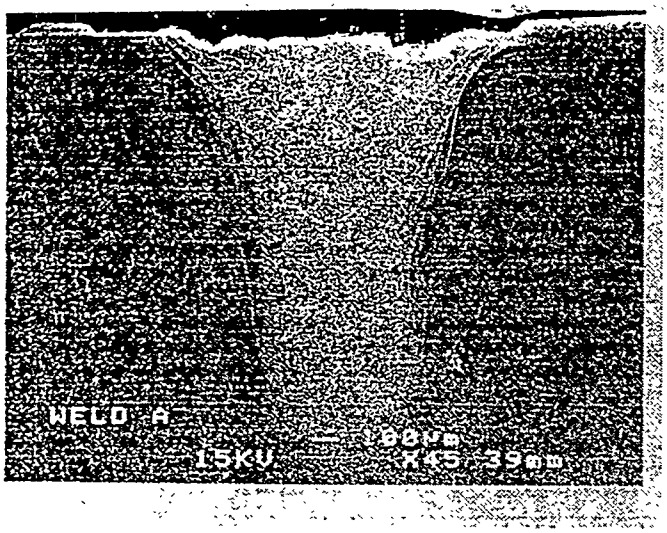

Figure 2. Scanning electron photomicrograph of Group II weldment AP.

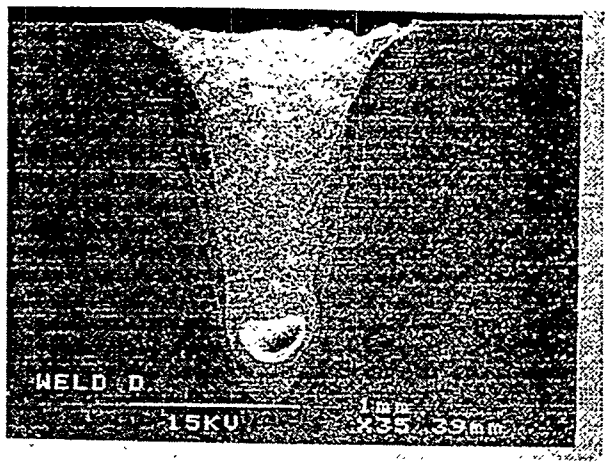

Figure 3. Scanning electron photomicrograph of Group II weldment DP.

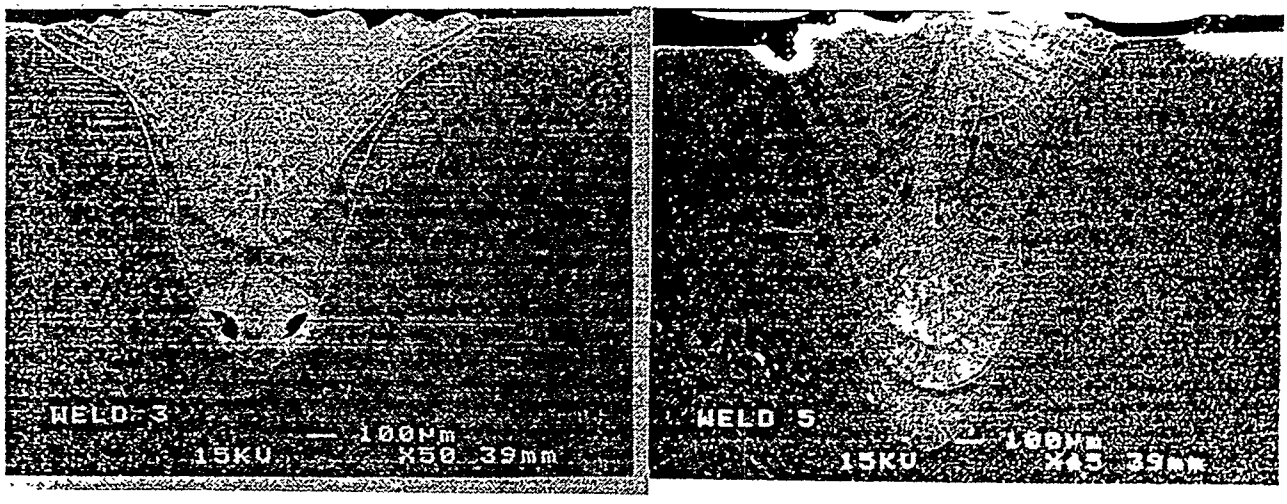

Figure 4. Scanning electron photomicrographs of Group II weldments 3P (left) and 5P (right).

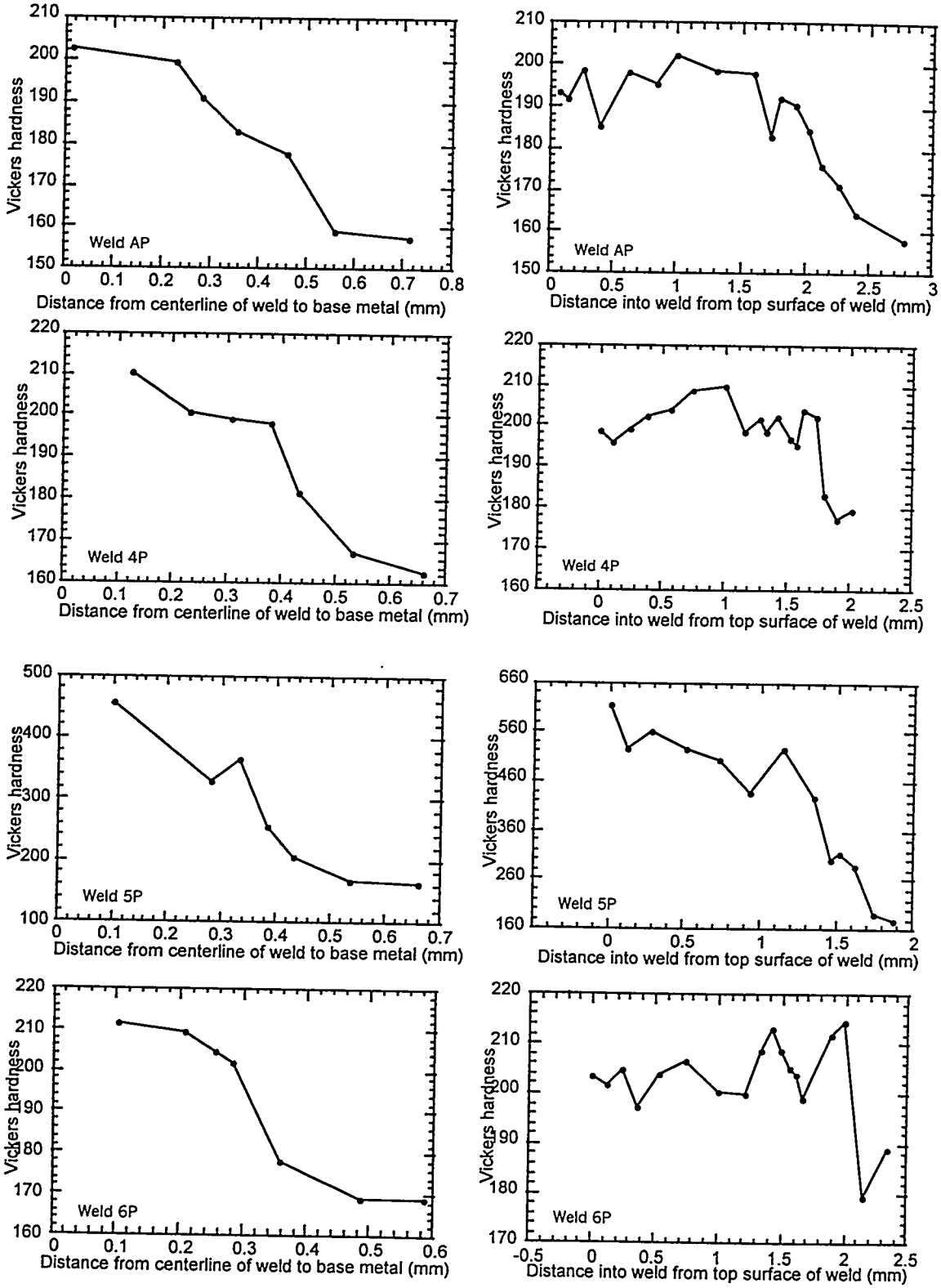

Figure 5. Vickers hardness profiles for Group II weldments AP, 4P, 5P, and 6P in surface-to-root direction and from weld centerline-to-base metal at half-width of weldment.

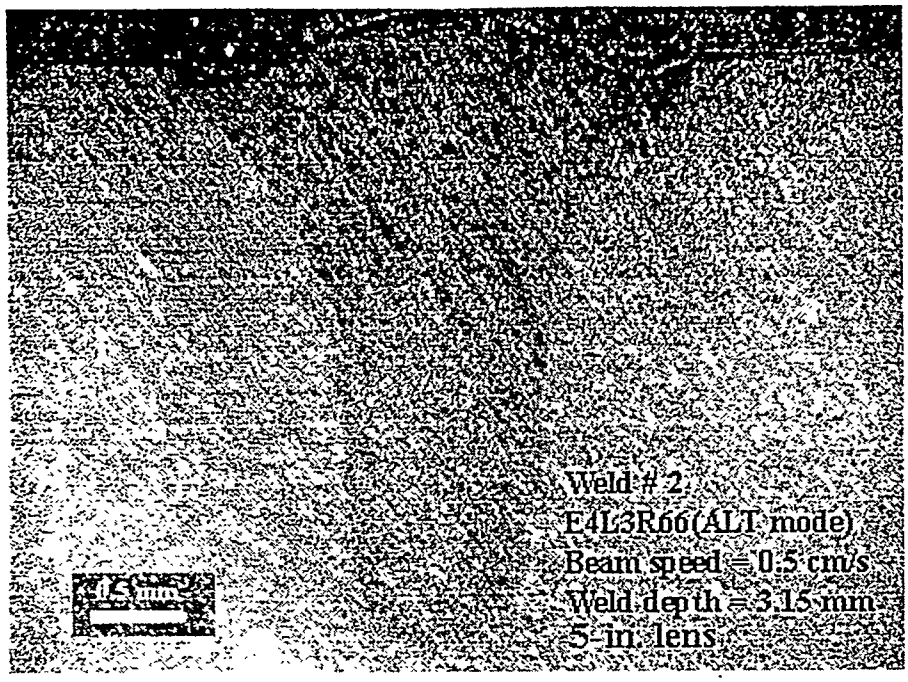

Figure 6 An ideal Group III weld produced under laser schedule of E4L3R132 and beam travel speed of 0.5 cm/s using a 127mm (5") lens.

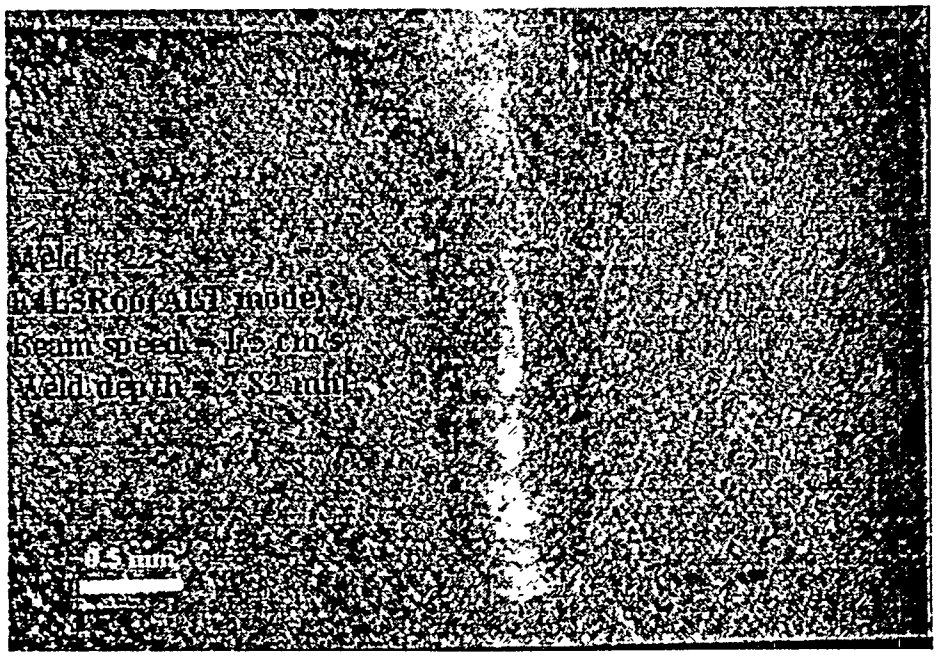

Figure 7 An ideal Group III weld produced under laser schedule of E4L3R132 and beam travel speed of 1.5 cm/s using a 76mm (3") lens.

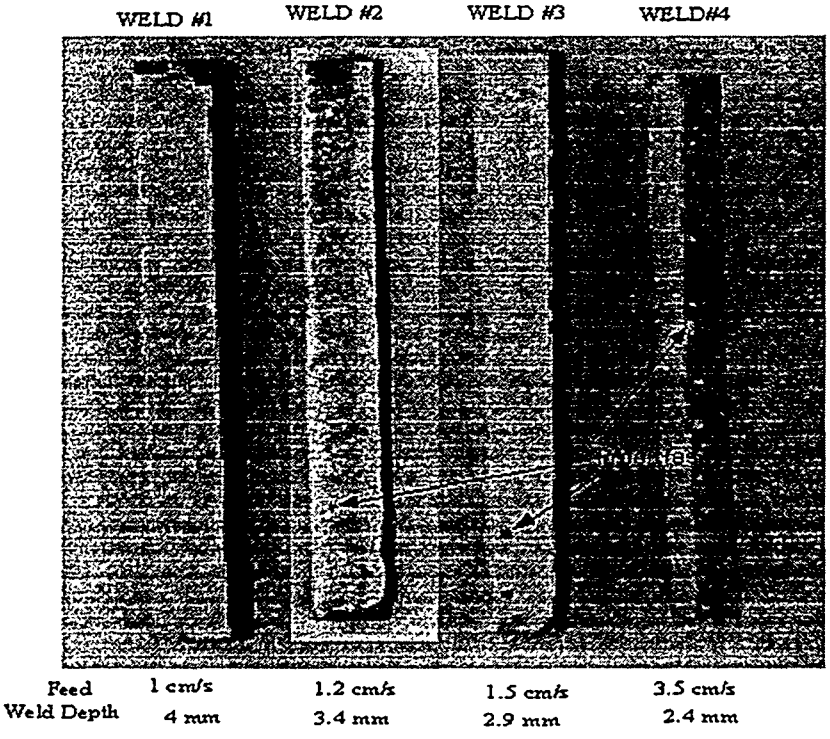

Figure 8. Longitudinal section views of laser-welded samples showing welds with porosity and a full penetration weld without porosity

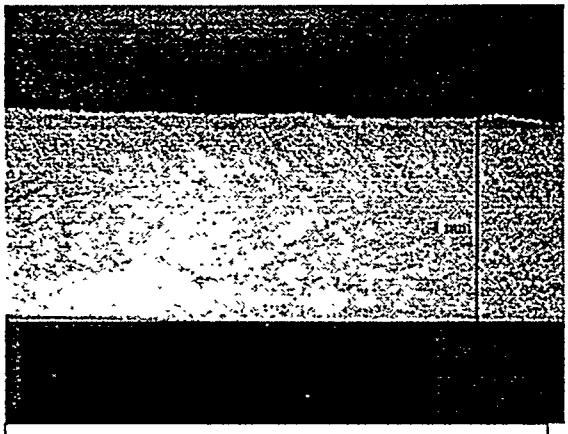

Figure 9. Closeup of longitudinal section view of weld No. 1 in Table 5.

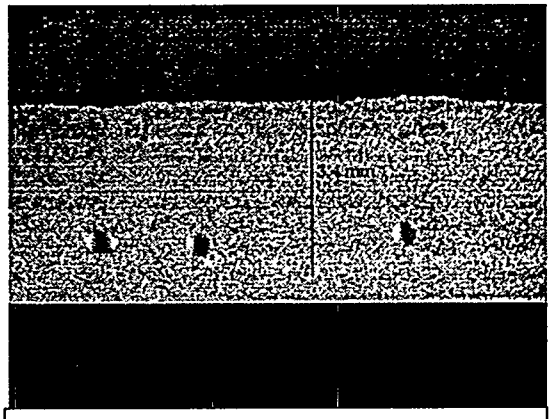

Figure 10. Closeup of longitudinal section view of weld No. 2 in Table 5.

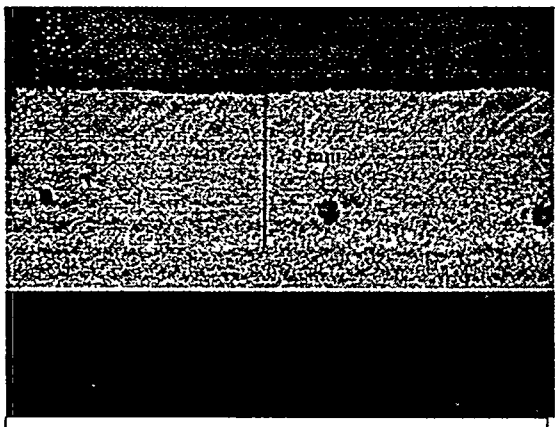

Figure 11. Closeup of longitudinal section view of weld No. 3 in Table 5.

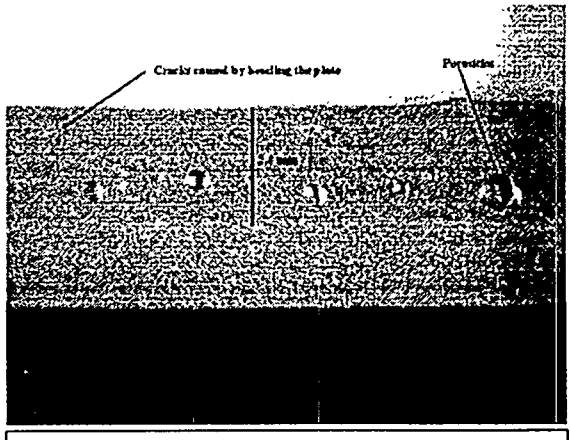

Figure 12. Closeup of longitudinal section view of weld No. 4 in Table 5.

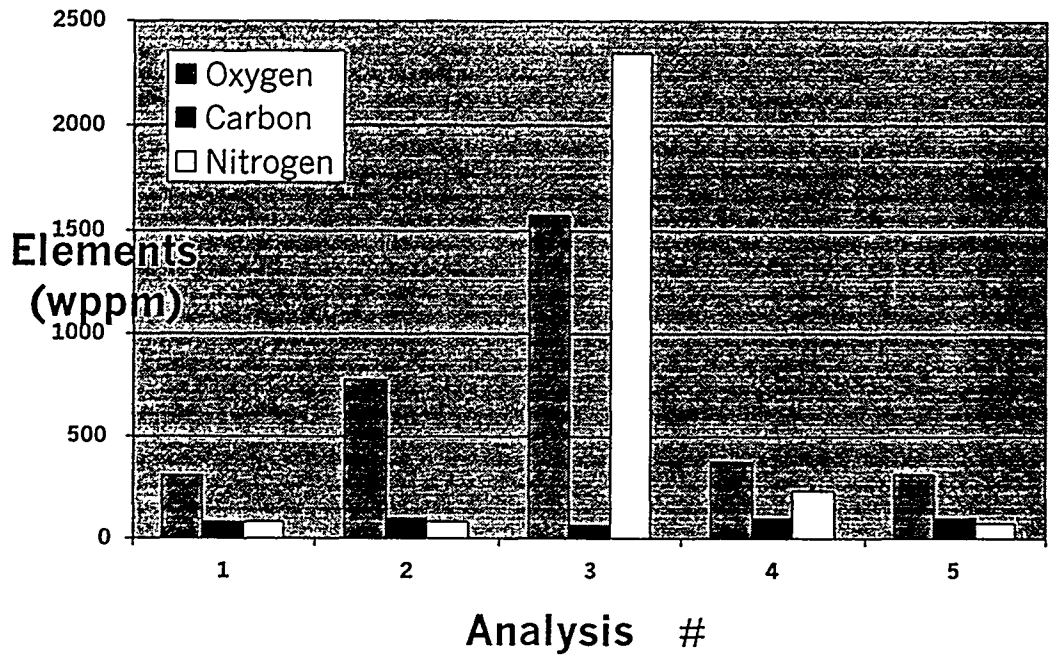

Analysis #	Specimen #	Welding Conditions	Lens	Beam travel speed (cm/s)	Sample form
1	Heat 832665	Reference Heat Analysis	-	-	-
2	23A	Base material	-	-	Chips
3	23B&23C	No ECB	76mm	1	Chips
4	09A&09B	ECB, Non-optimal gas flow	127mm	0.6, 0.5	Bar
5	12B&12C	ECB+ Optimal gas flow	127mm	0.4, 0.25	Bar

Figure 13. Chemical analysis results of laser welded V-Cr-Ti alloy samples from Group V welds.

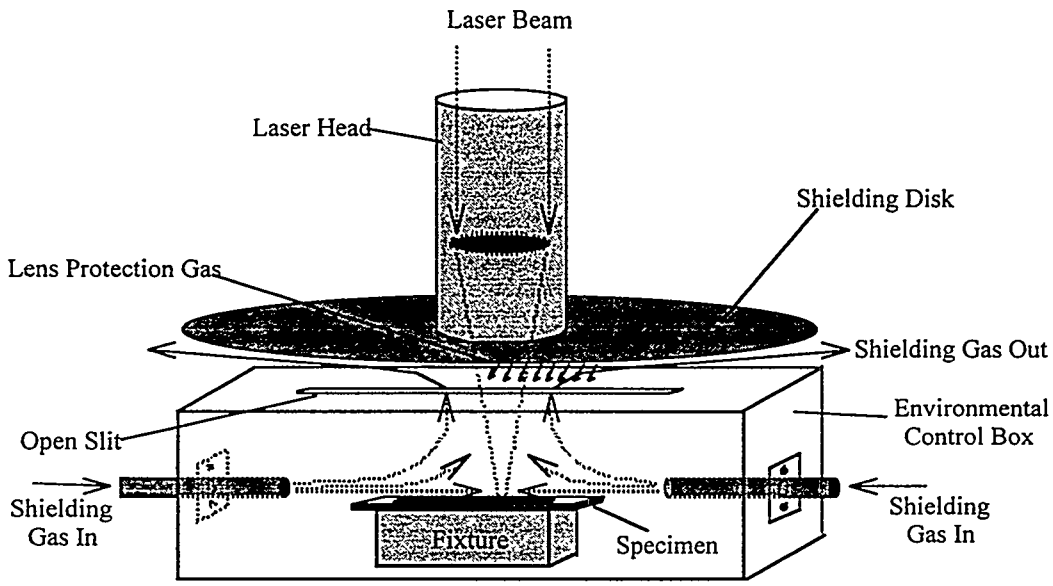

Figure 14. Set-up of the Environmental Control Box (ECB) for the laser welding system.

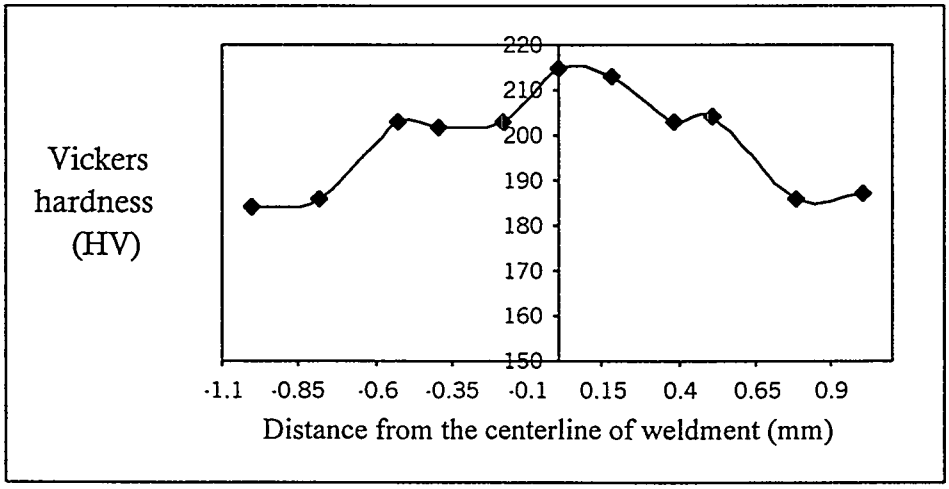

Figure 15. Microhardness profile for oxygen-uptake-free weldment Group V 12D (equivalent to 12C) at half-width of weldment.

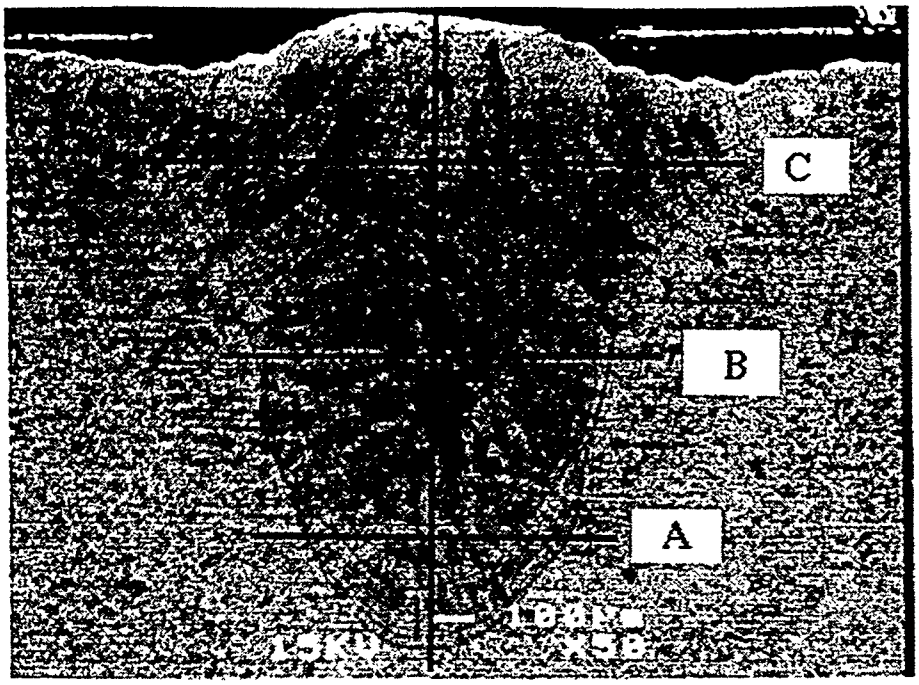

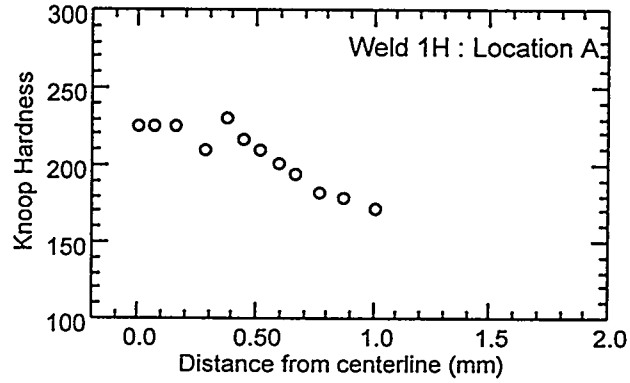

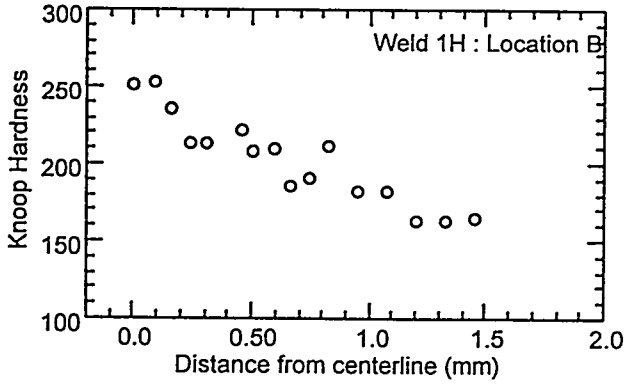

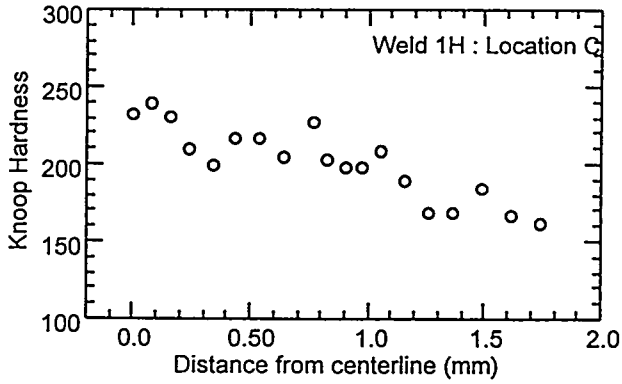

Figure 16. Hardness profiles at several elevations indicated in photomicrograph for laser-welded V-4Cr-4Ti specimen after post-welding treatment, designated as Weld 1H in Tables 1 and 6.

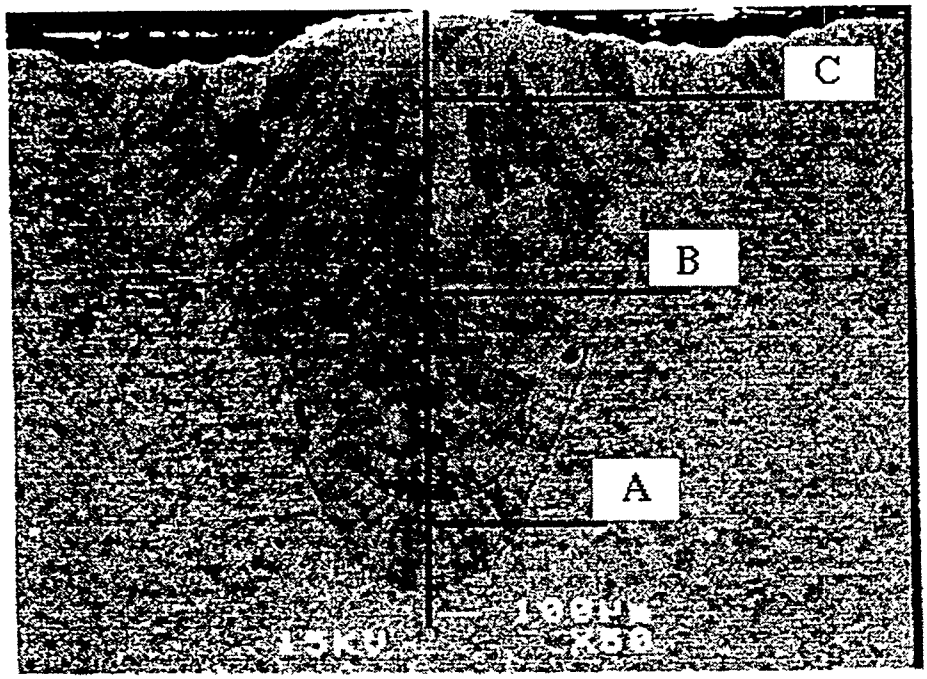

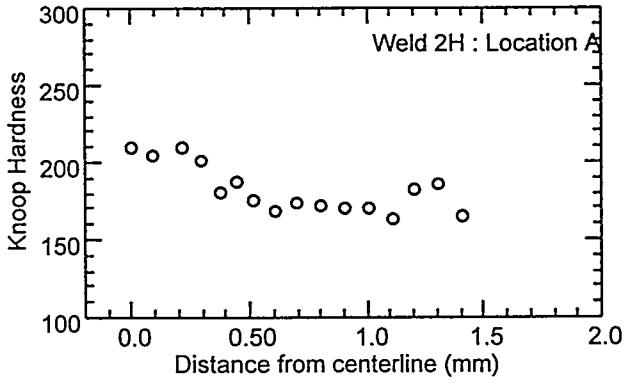

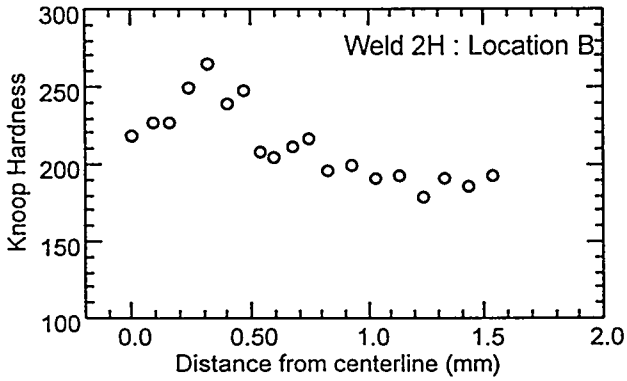

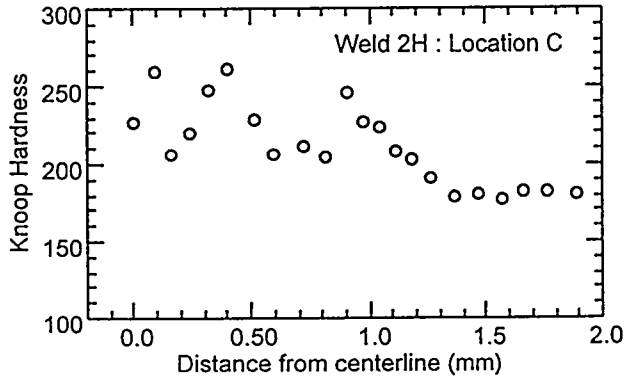

Figure 17. Hardness profiles at several elevations indicated in photomicrograph for laser-welded V-4Cr-4Ti specimen after post-welding treatment, designated as Weld 2H in Tables 1 and 6.

Table 1. Laser welding parameters for Group I welds (1H-7H), which were subsequently heat treated. Welding was performed with a 127 mm (5") lens.

Schedule E/L/R*	Focal Position	Weld ID	Feed (cm/s)	DOP** (mm)	Porosity ***
4/3/132	1 mm into	1H-7H	11	~1.4	NONE

* The meanings of the E/L/R in the laser Schedule for Tables 1-5, are as follows:
E: energy per unit time in joules/millisecond,
L : the pulse width in milliseconds and
R: the repetition rate in Hz or Pulses per second.
** **DOP** = Depth of Penetration
***Porosity was examined at a single, randomly selected cross section via 400X optical microscope.

Table 2. Laser welding parameters for Group II welds, 76 mm (3") lens.

Schedule E/L/R*	Focal Position	Weld ID	Feed (cm/s)	DOP** (mm)	Porosity ***
4.5/3/118	1 mm into	6P	3	1.59	ALMOST NONE
		5P	3	1.78	ALMOST NONE
		4P	3	1.65	ALMOST NONE
		3P	4	1.26	Y
		2P	4	1.37	Y
		1P	4	1.26	Y
5.2/3/102	1 mm into				
		AP	3	1.80	ALMOST NONE
		BP	2	2.46	Y
		CP	2.5	2.23	Y
5.5/3/96	1 mm into				
		DP	2.5	2.23	Y

Table 3. Laser welding parameters for Group III welds, 127mm (5") lens.

Schedule E/L/R*	Focal Position	No. of Welds	Feed (cm/s)	DOP** (mm)	Porosity ***	Irregular splatter	Ideal Weld
4/3/132	@ Surface	2	0.5	3.15-3.42			Y
		4	1	2.53-2.91		1/4	Y
		4	1.5	2.26-2.53	Y		
		1	2	1.86			
6/2/132	@ Surface						
		1	1.5	2		Y	
		1	2	1.17		Y	
4/3/132	1/2 mm into						
		1	2	1.48			
5/2.5/128	@ Surface						
		1	1.5	2.54	Y		
		2	2	1.89-1.94		Y	
4/2/200	1 mm into						
		1	1.5	2.02		Y	
4/3/132	1 mm into						
		1	1.5	2.2			
		1	1.8	2.17	Y		
		1	2	2.16	Y		

Table 4. Laser welding parameters for Group III welds, 76mm (3") lens.

Schedule E/L/R*	Focal Position	No. of Welds	Feed (cm/s)	DOP** (mm)	Porosity ***	Irregular splatter	Ideal Weld
4/3/132	**1 mm into**						
		1	1.5	2.82			Y
		1	2	2.81	Y		
		1	3	1.75			
		1	4	1.66			
5/3/106	**1 mm into**						
		1	2	2.43			
		1	2.5	2.5	Y	Y	
		1	3	1.79			
5.2/3/102	**1 mm into**						
		1	2	2.8	Y		Y
		1	2.5	2.37	Y		
		1	3	2.18			
5.5/3/96	**1 mm into**						
		1	2.5	2.5	Y	Y	
		1	3	1.92		Y	

Table 5. Laser welding parameters for Group IV welds, 76 mm (3") lens.

Schedule E/L/R*	Focal Position	Weld ID	Feed (cm/s)	DOP** (mm)	Porosity †	Irregular splatter	Ideal Weld
4/3/132	**1 mm into**						
		1	1	4			Y
		2	1.2	3.4	Y		
		3	1.5	2.9	Y		
		4	3.5	2.4	Y		

† Welds were EDM wire cut longitudinally along the centerlines of the welds to comprehensively examine for porosity.

Table 6. Laser heat treatment parameters of Group I welds.

Schedule E/L/R*	Focal Position	Weld ID	Feed (cm/s)	Ave. Power kW	Number of passes
4/3/132	26 mm into	1H	1	1325	1
		2H	1	1325	5
0/0/0 (NONE)					
		3H	-	0	0
2/2/200	26 mm into				
		4H	0.25	664	1
		5H	0.25	664	5
2/2/50	26 mm into				
		6H	0.25	319	1
		7H	0.25	319	5

DISTRIBUTION LIST FOR ANL/TD/TM00-13

Internal

S. Bhattacharyya
M. Billone
Y. Chang
P. Finck
Y. Gohar
S. Majumdar
R. Mattas
K. Natesan (3)
J.-H. Park
R. Poeppel
C. Reed (3)
W. Shack
D.L. Smith (3)
H. Tsai
Z. Xu (3)
TIS Files
FPP Files (10)

External

DOE/OSTI, for distribution (2)
ANL-E Library
ANL-W Library
K. Abe, University of Tohoku, Japan
C. Baker, University of California, San Diego, CA
S. Berk, U.S. Department of Energy, Germantown, MD
E. E. Bloom, Oak Ridge National Laboratory, Oak Ridge, TN
V. Chernov, Bochvar Research Institute of Inorganic Materials, Moscow, Russia
B. Chin, Auburn University
J. Davis, Boeing, St. Louis
W. Dove, U.S. Department of Energy, Germantown, MD
L. El-Guebaly, University of Wisconsin, Madison, WI
V. Evtikhin, State Enterprise Red Star, Moscow, Russia
O. Filatov, Efremov Scientific Research Institute, St. Petersburg, Russia
M. Fuetterer, CEA, Gif-sur-Yvette, France
M. Gasparotto, ENEA, Frascati, Italy
L. Giancarli, CEA, Gif-sur-Yvette, France
M. Grossbeck, Oak Ridge National Laboratory
R. Goldston, Princeton Plasma Physics Laboratory, Princeton, NJ
I. Kirillov, Efremov Scientific Research Institute, St. Petersburg, Russia
G. Kulcinski, University of Wisconsin, Madison, WI
R. Kurtz, PNNL
T. Kuroda, Japan Atomic Energy Research Institute, Naka, Japan
G. Lucas, University of California, Santa Barbara, CA
I. Lyublinski, State Enterprise Red Star, Moscow, Russia

S. Malang, Forschungszentrum Karlsruhe, Karlsruhe, Germany
W. Marton, U.S. Department of Energy, Germantown, MD
Y. Martynenko, Kurchatov Institute, Moscow, Russia
R. Matera, URC-IHCP, Ispra, Italy
S. Matsuda, Japan Atomic Energy Research Institute, Naka, Japan
H. Matsui, Tohoku University, Sendai, Japan
K. McCarthy, Idaho National Engineering and Environmental Laboratory, Idaho Falls, ID
R. Miller, University of California, San Diego, CA
T. Muruga, NIFS, Japan
R. Moir, Lawrence Livermore National Laboratory, Livermore, CA
S. Molokov, Coventry University, Coventry, United Kingdom
F. Najmabadi, University of California, San Diego, CA
R. Odette, University of California, Santa Barbara
R. Nygren, Sandia National Laboratories, Albuquerque, NM
R. Parker, Massachusetts Institute of Technology, Cambridge, MA
D. Petti, Idaho National Engineering and Environmental Laboratory, Idaho Falls, ID
J. Reimann, Forschungszentrum Karlsruhe, Karlsruhe, Germany
A. Rowcliffe, ORNC
M. Sawan, University of Wisconsin, Madison, WI
K. Schultz, General Atomic, San Diego, CA
G. Shatalov, Kurchatov Institute of Atomic Energy, Moscow, Russia
Yu.A. Sokolov, Minatom, Moscow, Russia
M. Solonin, Bochvar Research Institute of Inorganic Materials, Moscow, Russia
W.M. Stacey, Georgia Institute of Technology, Atlanta, GA
D. Steiner, Rensselaer Polytechnic Institute, Troy, NY
Y. Strebkov, Research and Development Institute of Power Engineering, Moscow, Russia
I. Sviatoslavsky, University of Wisconsin, Madison, WI
H. Takatsu, Japan Atomic Energy Research Institute, Tokyo, Japan
T. Terai, University of Tokyo, Tokyo, Japan
M. Tillack, University of California, San Diego, CA
M. Ulrickson, Sandia National Laboratories, Albuquerque, NM
J. Van der Laan, NRG, Petten, Netherlands
R. Van der Schaaf, NRG, Petten, Netherlands
J. Vetter, Forschungszentrum Karlsruhe, Germany
F.W. Wiffen, U.S. Department of Energy, Germantown, MD
C. Wong, General Atomics, San Diego, CA
S. Zinkle, Oak Ridge National Laboratory, Oak Ridge, TN
Bibliothek, Max-Planck-Institute fur Plasmaphysik, Germany
C.E.A. Library, Fontenay-aux-Roses, France
Librarian, Culham Laboratory, England
Thermonuclear Library, Japan Atomic Energy Research Institute, Japan